Research Square

Preprints are preliminary reports that have not undergone peer review.
They should not be considered conclusive, used to inform clinical practice,
or referenced by the media as validated information.

Calibration of the local magnitude scale (Ml)for Central Southern Africa

Blessing T Shumba (blessing@isc.ac.uk)
International Seismological Centre
Vunganayi Midzi
Council for Geoscience
Brassnavy Manzunzu
Council for Geoscience
Joseph R Maritinkole
Botswana Geoscience Institute

Research Article

Keywords: Wood-Anderson seismogram, Local magnitude scale, Amplitude, Seismic attenuation, Central Southern Africa

Posted Date: January 17th, 2023

DOI: https://doi.org/10.21203/rs.3.rs-2440171/v1

License: This work is licensed under a Creative Commons Attribution 4.0 International License.
Read Full License

Additional Declarations: No competing interests reported.

Version of Record: A version of this preprint was published at Journal of Seismology on March 21st, 2023. See the published version at https://doi.org/10.1007/s10950-023-10139-7.

Calibration of the local magnitude scale (M_l) for Central Southern Africa

Blessing T Shumba[1*], Vunganayi Midzi[2], Brassnavy Manzunzu[2] and Joseph R Maritinkole[3]

[1*]International Seismological Centre, Pipers Lane, Thatcham, RG19 4NS, UK.

[2]Engineering and Geohazards Uni, Council for Geoscience, Silverton, Pretoria, South Africa.

[3]Botswana Geoscience Institute, Lobatse, Botswana.

*Corresponding author(s). E-mail(s): blessing@isc.ac.uk;

Contributing authors: vmidzi@gmail.com; bmanzunzu@gmail.com; jrmaritinkole@gmail.com;

Abstract

The Central Southern Africa is an area of moderate seismic activity generally caused by the presence of the East Africa Rift System. To improve the quantification of seismicity in this region, we propose a local magnitude scale ($\boldsymbol{M_l}$), based on the original Richter definition to be used by the Zimbabwe and Botswana national networks. The magnitude scale is developed using 854 seismic events that occurred between 1997 – 2000 and 2013 – 2018. These events were recorded by 61 broadband seismic stations located in Botswana, Zimbabwe, and South Africa. We evaluated 6128 traces of zero to peak maximum amplitude, recorded on the horizontal channel from simulated Wood-Anderson seismograms. All

6128 maximum amplitude measurements were inverted simultaneously to determine the attenuation constants. The resultant $\boldsymbol{M_l}$ is defined as

$$\boldsymbol{M_l = \log_{10} A + 0.80 \times \log_{10}(R) + 0.00086 \times R - 1.37 \pm S}$$

in which $\boldsymbol{A}$ is ground displacement amplitude determined from instrument corrected synthetic Wood-Anderson seismograms in nanometres, $\boldsymbol{R}$ is the epicentral distance (km), and $\boldsymbol{S}$ is the station correction. Station corrections were determined for all stations during the regression analysis resulting in values ranging between -0.44 to + 0.31. The range in station corrections suggests a strong influence of local site effects on the amplitude of the seismic signal. Without station correction, the overall standard deviation of the magnitude residuals using our magnitude relation is 0.32 with a variance of 0.10, while using station corrections, the standard deviation and variance improved to 0.17 and 0.02 respectively. There is 80 % reduction in variance when our relation is used together with station corrections. A comparison of our local magnitude relation with published $\boldsymbol{m_{blg}}$ relationships for Southern Africa shows that these two magnitude scales are almost equivalent. The $\boldsymbol{M_l}$ equation for Central Southern Africa derived in this study has good correlation with $\boldsymbol{m_b}$ values reported by the ISC and NEIC and attains systematically lower magnitude values than the South African relationship.

Keywords: Wood-Anderson seismogram, Local magnitude scale, Amplitude, Seismic attenuation, Central Southern Africa

Article Highlights:

- Local magnitude scale was developed for Central Southern Africa region.
- The new scale will help in developing more accurate homogenized earthquake catalog for Botswana and Zimbabwe.
- The new scale will also improve seismic hazard studies Central Southern Africa.

1 Introduction

Local magnitude scale (M_l) is one of the commonly used scales to quantify relative size of an earthquake. It was defined by Richter(1935, 1958) as the logarithm of the maximum zero to peak amplitude measured on a Wood-Anderson (WA) instrument with amplification of 2800 at a natural period of 0.8 sec (Anderson and Wood, 1925). Some recent studies (Uhrhammer and Collins, 1990; Uhrhammer et al, 1996), as does the IASPEI standard formula (Bormann and Dewey, 2012) have shown that the effective amplification of the typical WA seismograph is around 2080 times. A standard formulation of Richter's M_l is written as (Richter, 1935, 1958; Hutton and Boore, 1987):

$$M_l = logA - logA_0 + S \tag{1}$$

Where, A is half of the peak-to-peak amplitude (mm) of a horizontal component on a standard WA seismometer, $-logA_0$ is the distance normalizing term that reflects the overall attenuation attributes in the region of interest, and S is the station correction defined relative to a reference site condition. In order to maintain (Richter, 1935) original definition of M_l, $-logA_0$ is defined such that 1 mm of amplitude on a WA instrument located at a reference site 100 km away from an event would register as a magnitude 3 event. The main aim of this study is to propose a relationship that estimates M_l from the inversion of amplitudes of earthquakes recorded by broadband seismic stations located in Botswana, Zimbabwe, and South Africa. Results from this study will improve the calculation of earthquake magnitudes in the region. The study area is characterized by a moderate level of seismicity. Although, the area experiences, low-magnitude seismicity, one large shallow earthquake occurred on the

3^{rd} of April 2017 with a magnitude M6.5 (Asefa and Ayele, 2021; Gardonio et al, 2018; Midzi et al, 2018). This earthquake was followed by aftershocks which lasted for several months (Mulabisana et al, 2021; Olebetse et al, 2020; Midzi et al, 2018). Monitoring of earthquakes in this area is carried out by the Botswana Geoscience Institute (BGI, formally the Botswana Geological Survey), Goetz Observatory (Department of Meteorological Services) in Zimbabwe and also by the Council for Geoscience (CGS), South Africa. Seismic monitoring in Zimbabwe started in 1959 through the installation of the first seismic station in Bulawayo. The need to establish a seismic network in Zimbabwe was necessitated by the building of the world's largest man-made lake in Kariba. The current network is made up of four broadband seismic stations. One of these stations (BLWY) is operated by Africa Array (AF). In addition, MATP seismic station was installed in 2004 as part of the International Monitoring System (IMS) network. In 2014, Goetz Observatory installed 2 more seismic stations at Chipinge (CHIPN) and Karoi (KRI) to add to the existing stations.

Since April 1993 a global telemetered seismograph station (LBTB), located in Lobatse, has been operating in Botswana. From November 2013 to February 2018, a temporary array of seismic stations (Network of Autonomously Recording Seismographs (NARS), Botswana network) was deployed in Botswana to address the questions about the crustal and upper mantle structure. The NARS consisted of 21 broadband seismic stations distributed over the whole country. In February 2018, following the 3^{rd} April 2017 M6.5 earthquake, the BGI converted the 21 temporary NARS stations to become part of the permanent network, which is now used to monitor earthquakes in and around Botswana. Data that is recorded from these stations is transmitted in real time to the

BGI for analysis. Between 1997 and 1999, the Southern African Seismic Experiment (SASE) was set up and broadband seismic stations were installed in Botswana, Zimbabwe and South Africa as part of this experiment. It was part of the Kaapvaal project (Carlson et al, 1996, 2000) with the responsibility to investigate the seismic structure of the region. Both BGI, Goetz Observatory and CGS use SEISAN (Havskov et al, 2020; Ottemöller et al, 2021) for manual analysis of local and regional earthquakes. BGI does not have its own magnitude relation and currently the South African M_l scale (Saunders et al, 2013) is used. This is assumed to be reasonable since the two areas are close and tectonically similar. The geology of South Africa and Zimbabwe are similar, they both consist of Archean cratons which are almost of similar age and the cratons are both surrounded by mobile belts (Eriksson et al, 2011; Fouch et al, 2004; Jelsma and Dirks, 2002)

During the 1963 — 1991 period, the m_{blg} magnitude scale was developed by Henderson (1974) and used for magnitude estimation in the southern African region by the Goetz Observatory. The Henderson (1974) relation (equation 2) assumes shallow focal depth between 0 and 10 km.

$$mb_{lg} = \log[A_{(\max)}/T] + \beta[\triangle] \tag{2}$$

in which $A_{(\max)}$ is the maximum ground motion amplitude of the Lg phase in μm, T is the period in seconds and the $\beta[\triangle]$ is the distance normalizing term. Further details of this relation are found in Chow et al (1980) and Hlatywayo (2001). The scatter in the derivation of $\beta[\triangle]$ in Henderson (1974) was large and in order to improve the magnitude values of earthquakes in Southern Africa, Chow et al (1980) developed an m_{blg} magnitude scale using a large dataset and obtained the following distance normalizing term

$$\beta(\triangle) = 2.66 \log_{10} \triangle + 2.61 \tag{3}$$

for

$$5^\circ \leq \triangle \leq 20^\circ$$

where $A_{(\max)}$ is the ground motion amplitude of the Lg phase in nanometres (nm) and $\triangle$ is the epicentral distance.

2 Data and Processing

Three component digital recordings from 61 seismological stations from Botswana, Zimbabwe, and South Africa, were used to carry out this study. These recordings correspond to shallow earthquakes of focal depth less than 35 km. Of the 61 stations used in this study, 20 are part of the SASE broadband seismic stations. Furthermore, we used seismic stations from NARS, BX – Botswana network and two Zimbabwean permanent stations. These stations continuously recorded earthquake data in that time period. Fig. 1 shows a map of stations as well as epicentral locations of the 854 earthquakes whose parameters were used in this study.

The reviewed standard earthquake Bulletin that is routinely released by the International Seismological Centre (ISC) (publicly available at http://www.isc.ac.uk) was used to select 854 events for which matching waveform data were obtained from the Incorporated Research Institutions for Seismology (IRIS). Fig. 2 shows the distribution of earthquakes used with respect to hypocentral distance. The analysis was restricted to earthquakes recorded in the range 0 – 1000 km from the hypocentre. Magnitudes in Fig. 2

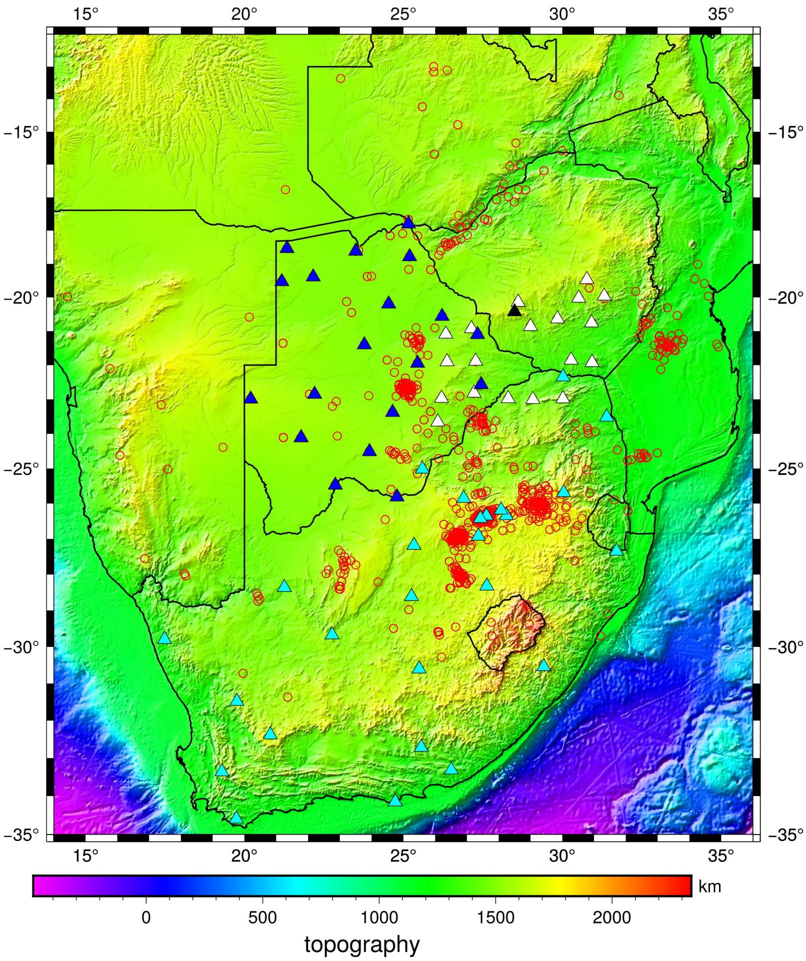

Fig. 1 Topographic map showing the spatial distribution of earthquakes (red open circles) used in this study. Dark blue triangles show the NARS stations while the white triangles are stations from the SASE network used in this study. The black triangle represents MATP station. The sky blue triangles represent stations used by the Council for Geoscience (CGS) in their routine data analysis (Saunders et al, 2013)

were calculated using the relationship obtained in this study. Fig. 2 also shows that most earthquakes used in this study are within the M_l range of 2–7.

To generate an M_l scale for Central Southern Africa, a Python-based algorithm was developed to automatically measure half peak-to-peak displacement amplitudes using the compiled waveform data. We took advantage of the software Obspy (Beyreuther et al, 2010), a Python-based package with several

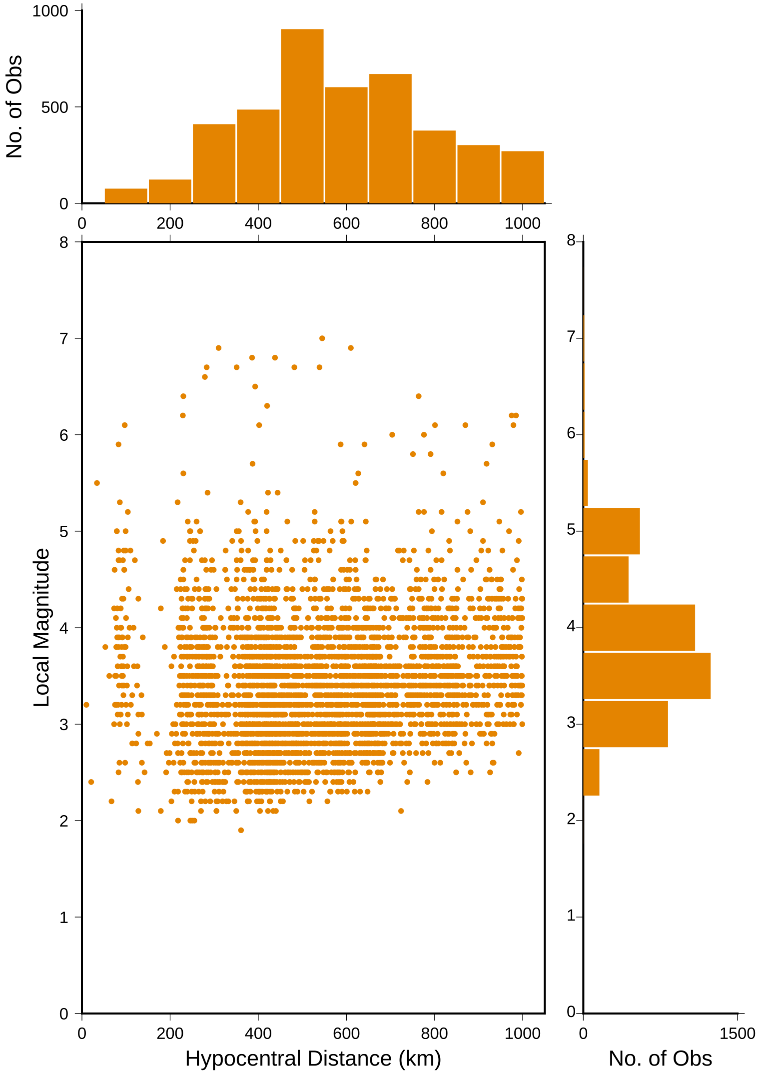

Fig. 2 Magnitude and hypocentral distance distribution for earthquakes used in this study. Event magnitudes are computed using the scale developed in this study.

modules designed to help users in the workflow of downloading, inspecting and processing of seismic waveforms. All waveform traces were demeaned, filtered between 1 and 10 Hz, and transformed to displacement through deconvolution of the instrument response. Given the location of an event as provided in the

ISC Bulletin, we used the AK135 velocity model (Kennett et al, 1995), to predict local P and S wave arrivals. We then applied a standard signal-to-noise ratio (SNR) detector around the predicted arrivals to check the quality of the waveforms (example of a processed waveform is shown in Fig. 3).

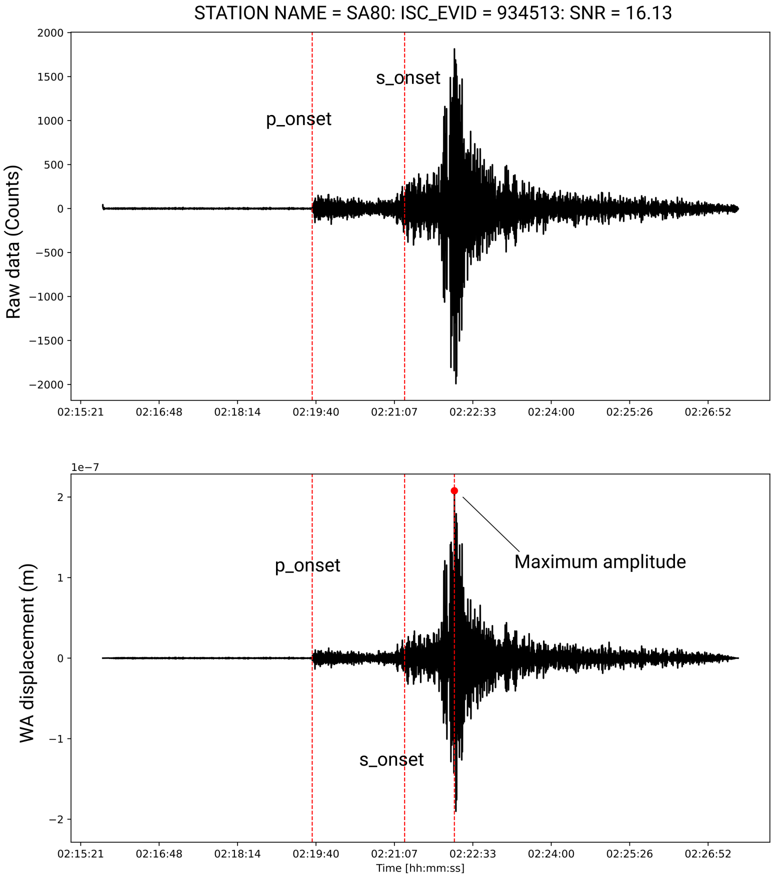

Fig. 3 Regional earthquake seismograph 1997/08/01 4.7 $m_{b(isc)}$ for an earthquake located in South Africa that was recorded by station SA80 in Zimbabwe at 8.97° from the epicentre. The top trace is the original record whilst the bottom trace is the simulated WA record. p_onset and s_onset are the theoretical P wave and S wave arrival times respectively.

We performed several tests on the SNR to identify the best minimum threshold. In this study we define the threshold to be 2.0, thus waveforms with

$SNR \leq 2.0$ were rejected. For each station and for each earthquake, maximum trace amplitudes were measured on both N-S and E-W components. The absolute maximum amplitude between the 2 components was used to constitute a single measurement. The automatically measured amplitudes at most seismic stations compared favourably to amplitudes that are stored at the ISC Bulletin (e.g Fig. S1). Our approach for amplitude picking, described above is summarized in the flowchart in Fig. S2. The number of observations made at each seismic station are shown in Fig. 4a and amplitudes picked are plotted against hypocentral distance as shown in Fig. 4b.

In order to develop the M_l scale for Central Southern Africa, we applied the general form of local magnitude scale by (Richter, 1935) as follows:

$$M_{l(ij)} = \log_{10} A_{ij} + a \log_{10} R_{ij} + bR_{ij} + S_j + C \tag{4}$$

where $_i$ and $_j$ are earthquake and station index respectively. The coefficient a, depends on geometrical spreading, b on attenuation, A_{ij} is amplitude measured in nanometres (nm), R_{ij} is the hypocentral distance in km, S_j is the station correction to the magnitude for the j^{th} observation site and C is a station correction term which gives the same magnitude for the same amplitude at the reference distance as in Southern California (Richter, 1935). We invert for a and b using singular decomposition method as implemented in the MAG2 program which is part of the SEISAN software package Ottemöller and Sargeant (2013); Havskov et al (2020); Ottemöller et al (2021). MAG2 utilizes singular value decomposition (SVD) using Numerical Recipes (Press et al, 1996) to invert the observations. Furthermore, we also conducted another inversion in which a, and b values are fixed to the scale we obtained, and only invert for the station corrections. Table 1 represents the input parameters that were used with the

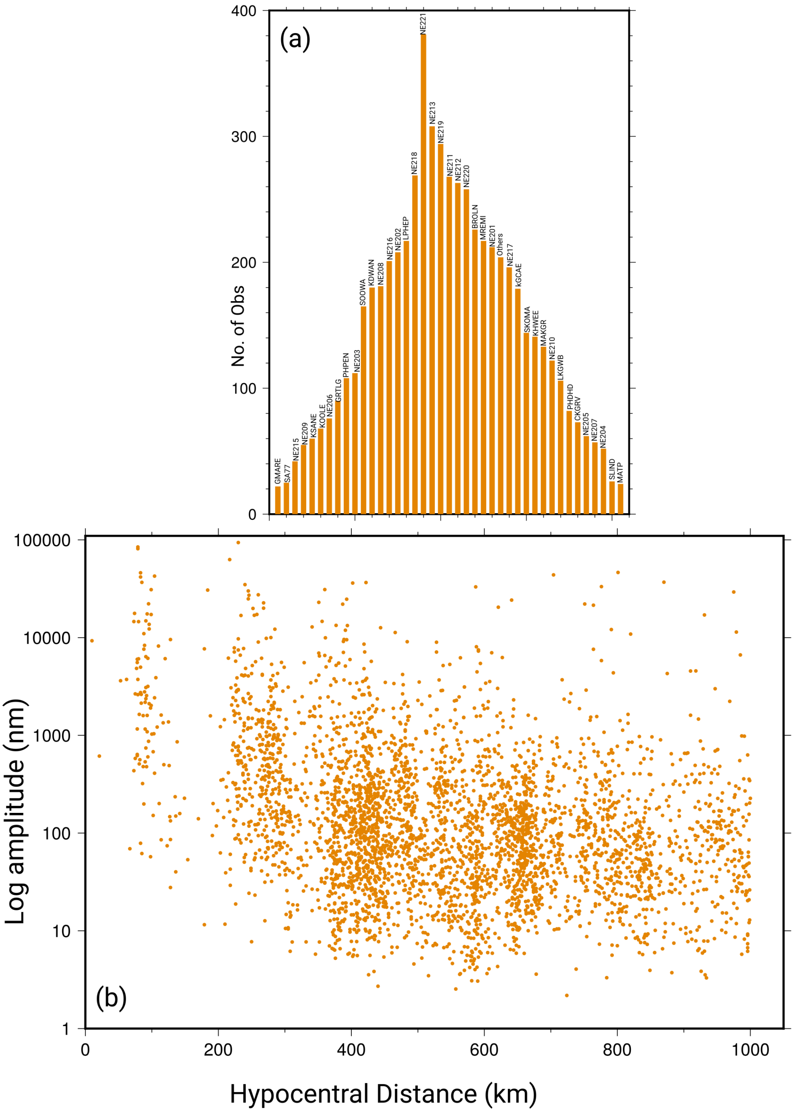

Fig. 4 **(a)** Number of station readings used in analysis **(b)** Logarithm of the WA amplitudes in nm as a function of distance.

MAG2 code. We calculated magnitude residuals between magnitude assigned to a single station and the median magnitude earthquake. The M_l values obtained using the new relation derived in this study were then compared to those obtained for the same events using the Saunders et al (2013) relation for South Africa, Hutton and Boore (1987) for California, and Ottemöller and

Sargeant (2013) scale for the United Kingdom. Furthermore, our M_l values were also compared to m_{blg} values which we calculated based on the Henderson (1974) and Chow et al (1980) relations.

Table 1 Input data to the mag2 code.

Input variable	**Value**
Minimum number of observations per event	5
Number of events used	854
Number of observations	6128
Number of stations	61
Number of equations for SVD inversion	5310
Number of model parameters	687
Distance range	$0 - 1000$ km

To evaluate whether the new scale is an improvement over any alternative relation, we look for a reduction in standard deviation (equation 5) and overall variance (equation 6) of all magnitude residuals computed as

$$\sigma = \sqrt{\sum \frac{(x_i - \mu)^2}{N}} \tag{5}$$

$$\sigma^2 = \sqrt{\sum \frac{(x_i - \mu)^2}{N - 1}} \tag{6}$$

in which σ is the standard deviation of all the observations, N is the number of all observations, x_i is the value of each observation, μ is the mean of all the observations and σ^2 is the variance of the observations.

3 Results and Discussion

The coefficients (a, b and C) were determined by applying the SVD using the Numerical Recipe routines (Press et al, 1996) to invert 6128 amplitude value observations. The corresponding epicentres-station path covers most of the studied areas in Botswana, South Africa and Zimbabwe (Fig. 5).

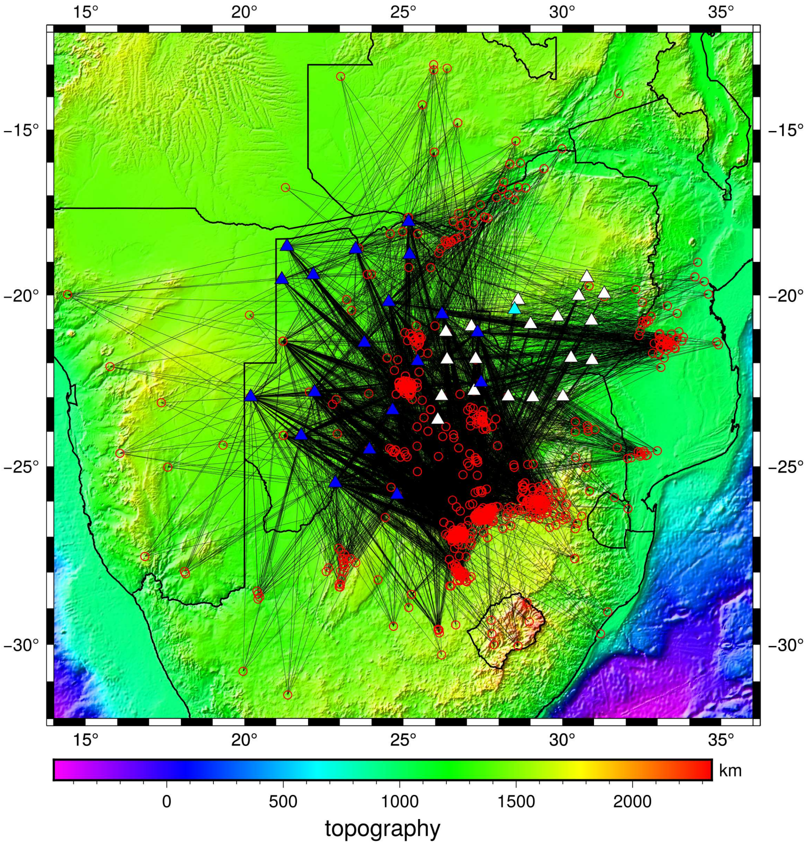

Fig. 5 Ray-Path coverage of 854 events used for M_l inversion. Red open circles give the event locations, dark blue triangles indicate NARS station locations, white triangles are SASE stations and sky blue triangle is the MATP station in Zimbabwe. The black lines represent epicentre-station path.

After inverting our observations, we obtained the following scale:

$$M_l = \log_{10} A + 0.80 \times \log_{10}(R) + 0.00086 \times R - 1.37 \pm S \qquad (7)$$

in which A is ground displacement amplitude determined from instrument corrected synthetic WA seismograms in nanometres, R is the hypocentral distance (km), and S is the station correction. The estimated value for the geometrical spreading coefficient, a, is 0.80 ± 0.24, and the anelastic attenuation coefficient, b, is 0.00086 ± 0.00025 and C is -1.37. The obtained M_l relation is valid for distances up to 1000 km.

Fig. 6 shows the comparison of our calibration curves against those for Southern California (Hutton and Boore, 1987), South Africa (Saunders et al, 2013) and United Kingdom (Ottemöller and Sargeant, 2013). It can be seen that for distances less than 80 km, the attenuation rate for Central Southern Africa is slightly larger than the (Saunders et al, 2013) relation, the (Hutton and Boore, 1987) relation and the relation by (Ottemöller and Sargeant, 2013). However, for all distances greater than 80 km, the attenuation obtained in this study is significantly lower than that of Southern California and the United Kingdom. This is not surprising since the geology of our study is dominated by old cratons which promote low seismic attenuation.

The station correction factor for a particular station represents the local site conditions (Richter, 1958) and can be used to compensate for heterogeneous velocity structure near affected stations (Douglas, 1967; Pujol, 1988). High station correction values indicate site effects related to geological conditions or the presence of seismic noise have a strong influence on amplitude.

Fig. 7 is a representation of mean station residual variation across different networks within the study area. As we have explained before, BX network is a continuation of the NARS network. The only difference between the two networks is that during the transition, the sample rate was changed from 20 Hz (NARS network) to 40 Hz (BX network).

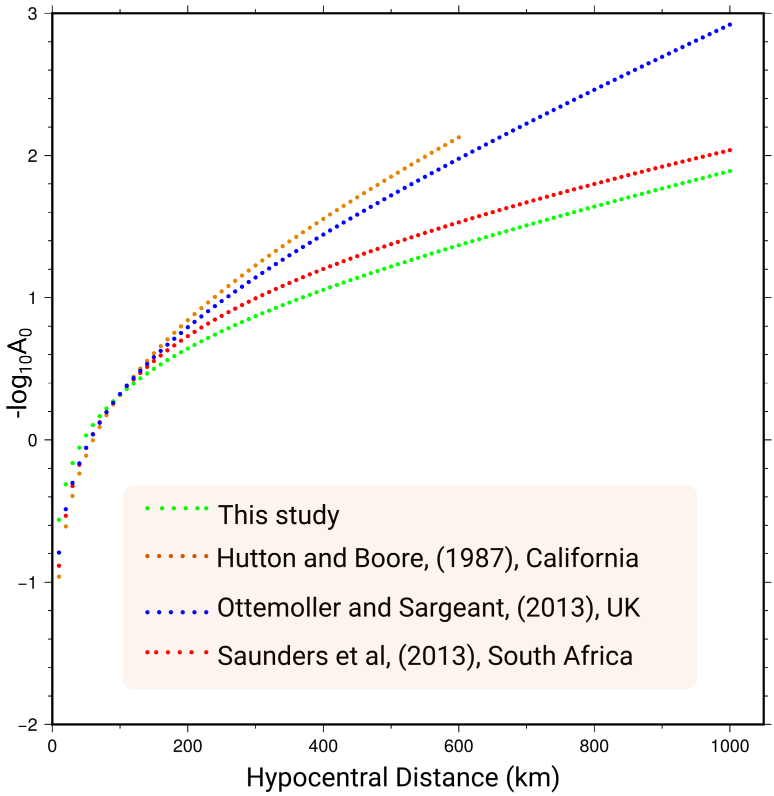

Fig. 6 Comparison of attenuation curves for Southern California, South Africa, United Kingdom (UK), Turkey and for the area of this study.

For the NARS and BX networks, stations are arranged such that the station below is a cosite station to the station above it. As an example, station NE201 is a cosite station to SKOMA and station NE213 is now station PHPEN. From Fig. 7, it can be seen that the two networks have similar station corrections. Also shown in Fig. 7 are the mean station residuals for cosite station BLWY an Africa Array (AF) station and SA72 from the SASE network. Station MATP is located at approximately 20 km south of station SA72/BLWY. As seen from Fig. 7, station SA72 has a low station correction and standard deviation. This is not surprising since it can be seen that almost all stations from the SASE network have consistently low station residuals as compared to the NARS and

BX networks. Furthermore, the station correction differences between SASE stations and BX/NARS network stations is clearly visible at some nearby sites such as NE220 and SA68 as well as NE217 and SA71. We are not sure as to why the SASE network has low station corrections but we can only speculate that this may be due to good metadata stored at IRIS. To sum up, station corrections calculated in this study range from -0.44 to +0.31.units of magnitude, which suggests significant differences in site effect.

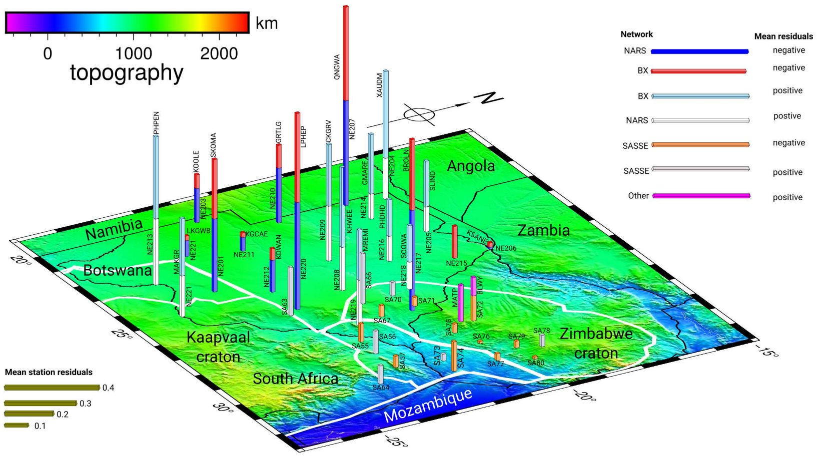

Fig. 7 Spatial variation of average station residuals (station magnitude-median magnitude) deduced in this study. Negative and positive average are shown by green and red colour, respectively. Text near the vertical bars denote seismic stations names. White polygons indicate the boundaries of the cratons inside our study area.

Fig. 8 shows comparison of our M_l with m_{blg} derived from Chow et al (1980), m_{blg} after Henderson (1974), $m_{(bISC)}$, $m_{(bNEIC)}$ and M_l reported by South Africa $M_{l(PRE)}$. To compare our relation withm_{blg}, we extracted Lg maximum amplitudes from the ISC Bulletin. These Lg amplitudes were then used to compute the m_{blg} magnitudes using relations after Chow et al (1980) and Henderson (1974). For $m_{b(ISC)}$, $m_{b(NEIC)}$ and $M_{l(PRE)}$, we downloaded network magnitudes from the ISC Bulletin (Storchak et al, 2017, 2020) and then compared the network magnitude with event magnitudes calculated in this study.

For our M_l and m_{blg} (Chow et al, 1980) we obtained a strong positive correlation of ($R^2 = 0.86$) from regression analysis using 100 entries. The relation between our Ml and mblg is shown in Equation 8:

$$m_{blg(Chow\ et\ al.,\ 1980)} = 0.80 \times M_l - 0.006, \tag{8}$$

for $m_{blg} \leq 5.9$, n =100

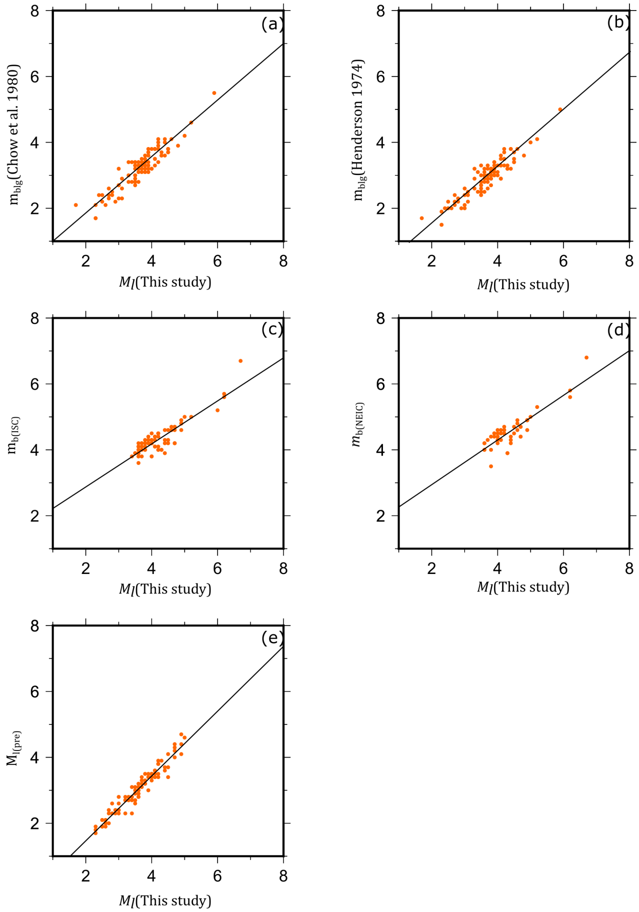

Fig. 8 Comparison of our local M_l obtained in this study plotted against **(a)** m_{blg} by Chow et al. (1980) **(b)** m_{blg} by Henderson (1974) **(c)** $m_{b(ISC)}$ **(d)** m_{bNEIC} **(e)** $M_{(lPRE)}$. In all figures, the solid black line represents the best-fit line obtained from the regression analysis.

Similarly, there is a good correspondence ($R^2 = 0.86$) between the Henderson (1974), m_{blg} and M_l from this study. We derived the following relation (equation 9).

$$m_{blg(Henderson,\ 1974)} = 0.85 \times M_l + 0.12, \tag{9}$$

for $m_{(blg)} \leq 5.9$, n =100

The correlation of our M_l and $m_{b(ISC)}$ from 90 entries as depicted in Fig. 9c is seen to follow the relation in equation 10,

$$m_{b(ISC)} = 1.08 \times M_l - 0.18, \tag{10}$$

for $m_{b(ISC)} \leq 6.7$,n =90, with a strong positive correlation. Similarly, the regression between $M_{l(thisstudy)}$ and $m_{b(NEIC)}$ as presented in Fig. 8d yielded the following relation (equation 11), where ($R^2 = 0.94$)

$$m_{b(NEIC)} = 0.65 \times M_l + 0.57, \tag{11}$$

for $m_{b(NEIC)} \leq 6.8$,n =84, with a positive correlation ($R^2 = 0.80$) Magnitude residuals, defined as the difference between the magnitude calculated at individual stations and the event magnitude for all the stations for a particular seismic event are shown in Fig. 9 and Table S1. The magnitude residuals obtained using the relation by Hutton and Boore (1987) with station corrections is shown in Fig. 9a. Similarly, Fig. 9b shows results obtained using the relation by Saunders et al (2013) with station corrections. Magnitude residuals obtained using the relation derived in this study without station corrections is shown in Fig. 9c and with station corrections in Fig. 9d. From Fig. 9, it is observed that there is less scattering in residuals for the newly developed magnitude scale with station corrections as compared to the residuals obtained using the other relations as well as the relation from this study without corrections. The overall, standard deviation of the magnitude residuals was computed to check the effect of the new magnitude relation on magnitude estimates. Summarised in Table 2 is the comparison of standard deviation and variance of the magnitude residuals, and it can be seen that the standard deviation σ of magnitude residuals from our study without stations correction is 0.32 (variance, $\sigma^2 = 0.10$). Similarly, with station correction, we obtained a standard deviation of 0.15 and variance of 0.02. These results show that the addition of station corrections reduces the variance by 80 % and this reduction of variance reduces station residuals close to zero. The standard deviation in residuals and variance for Saunders et al (2013) using station corrections is also quite low with values of 0.16 and 0.02 respectively. The average of the magnitude residual for different stations are shown in Fig. 9e for bin distances of 100 km, along with error bars. The residuals in Fig. 9e are small, which shows that the newly developed magnitude scale compensates attenuation effects for all distance ranges. Even though our new M_l scale with station corrections and the Saunders et al (2013) M_l scale with station corrections produce almost identical residuals a closer look at the number of observations (bar graph on right hand side in Fig. 9) indicates that the average residual of our results with station correction is close to zero compared to the Saunders et al (2013) relation. The geometrical spreading parameter and the distance attenuation parameter values are slightly different.

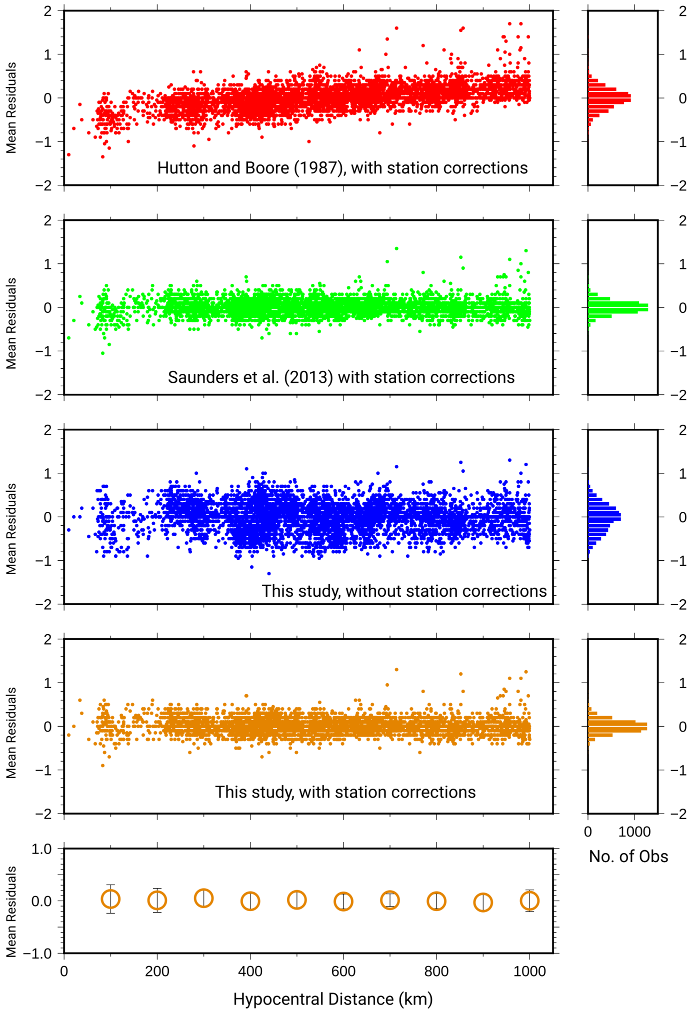

Fig. 9 Magnitude residuals calculated (a) (Hutton and Boore, 1987) with station corrections, (b) Saunders et al (2013) relation with station corrections (c) this study without station correction and (d) this study with station correction. (e) Mean values of magnitude residuals for the relation from this study with station corrections, divided in 100 km bins as a function of distance.

4 Conclusion

A local magnitude scale was derived for Central Southern Africa using 6128 traces of maximum amplitude observations. The observations were measured

Table 2 A comparison of the geometrical spreading parameter a, distance attenuation parameter b and standard deviation σ and variance σ^2 in magnitude residuals of the (Saunders et al, 2013) scale and the scale developed in this study.

Magnitude Scale	**a**	**b**	σ	σ^2
This Study (without station corrections)	0.80	0.00086	0.319	0.102
This Study (with station corrections)	0.80	0.00086	0.154	0.024
(Saunders et al, 2013) (with station corrections)	1.14	0.00063	0.156	0.024
(Hutton and Boore, 1987) (with station corrections)	1.11	0.00189	0.251	0.063

on the horizontal components of observed WA seismograms at distances ranging from 0 to 1000 km. The data used was obtained from records of 854 shallow earthquakes recorded by 61 broadband seismic stations. The scale derived was based on the Richter (1935) definition of M_l. As part of the inversion process, station corrections were determined for each of the stations that contributed data. Values determined range from -0.44 to +0.31. Magnitude values obtained using the new Central Southern Africa M_l scale were compared to those published by NEIC, PRE and ISC. The comparison shows that our solutions are stable and can replace the current M_l relation being used in the region. Results obtained were also analysed by studying the trend of the magnitude residuals. Overall, the standard deviation and variance of the magnitude residuals without using station corrections are 0.32 and 0.1 respectively while those obtained in this study using station corrections is 0.16 and 0.02. This shows 80 % reduction in variance indicating that using the new relation obtained in this study brings the average residual close to zero.

5 Data and resources

The bulletin data that was used in this study were downloaded from the ISC Bulletin (ISC, 2022). Waveform data were obtained from the Incorporated Research Institutions for Seismology (IRIS). The python package Obspy (Beyreuther et al, 2010) was used to obtain some of the waveform data. Most of the plots were generated using the Generic Mapping Tool (GMT) of (Wessel et al, 2019).

6 Acknowledgements

The authors based at the ISC are grateful to 72 Member-Institutions of the ISC in 47 countries (including NSF Awards 1811737) and approximately 150 parametric event data providers in 100 countries; they also thank several grantors and sponsoring organizations: the Comprehensive nuclear Test Ban Treaty Organization (CTBTO), FM Global, the Lighthill Risk Network, AXA XL, GeoSIG, SARA, and MS & AD InterRisk Research and Consulting.

7 Authors' contributions

Blessing Shumba contributed to the development of the concept, data analysis, interpretation, and report writing. Vunganai Midzi was instrumental in the concept development and report writing. Brassnavy Manzunzu was involved in the report writing. Joseph Maritinkole was involved in data collection.

8 Funding

No funding was obtained for this study

9 Competing interest

The authors declare that they have no known competing financial interests or personal relationships that could have influenced the work reported in this paper.

References

Anderson JA, Wood HO (1925) Description and theory of the torsion seismometer. Bulletin of the Seismological Society of America 15(1):1–72. https://doi.org/10.1785/BSSA0150010001

Asefa J, Ayele A (2021) Rupture process of the april 2017 mw 6.5 Botswana earthquake: deepest earthquake observed in continental africa. Arabian Journal of Geosciences 14. https://doi.org/10.1007/s12517-021-06890-1

Beyreuther M, Barsch R, Krischer L, et al (2010) Obspy: A python toolbox for seismology. Seismological Research Letters 81(3):530–533. https://doi.org/doi.org/10.1785/gssrl.81.3.530

Bormann P, Dewey JW (2012) The new iaspei standards for determining magnitudes from digital data and their relation to classical magnitudes. In: New manual of seismological observatory practice 2 (NMSOP-2). Deutsches GeoForschungsZentrum GFZ, p 1–44

Carlson R, Boyd F, Shirey S, et al (2000) Continental growth, preservation and modification in southern africa. GSA Today 10(2):1–7

Carlson RW, Grove TL, De Wit MJ, et al (1996) Program to study crust and mantle of the archean craton in southern africa. Eos, Transactions American Geophysical Union 77(29):273–277. https://doi.org/doi.org/10.1029/96EO00194

Chow R, Fairhead J, Henderson N, et al (1980) Magnitude and Q determinations in southern africa using lg wave amplitudes. Geophysical Journal International 63(3):735–745. https://doi.org/10.1111/j.1365-246X.1980.tb02648.x

Douglas A (1967) Joint epicentre determination. Nature 215(5096):47–48. https://doi.org/doi.org/10.1038/215047a0

Eriksson PG, Rigby MJ, Bandopadhyay P, et al (2011) The kaapvaal craton, south africa: no evidence for a supercontinental affinity prior to 2.0 ga? International Geology Review 53(11-12):1312–1330

Fouch MJ, James DE, VanDecar JC, et al (2004) Mantle seismic structure beneath the kaapvaal and zimbabwe cratons. South African Journal of Geology 107(1-2):33–44

Gardonio B, Jolivet R, Calais E, et al (2018) The april 2017 Mw6.5 Botswana earthquake: an intraplate event triggered by deep fluids. Geophysical Research Letters 45(17):8886–8896. https://doi.org/10.1029/2018GL078297

Havskov J, Voss PH, Ottemöller L (2020) Seismological observatory software: 30 yr of seisan. Seismological Research Letters 91(3):1846–1852. https://doi.org/10.1785/0220190313

Henderson N (1974) Earthquake magnitude determination based on short-period crustal waves. Department of Meteorological Services

Hlatywayo D (2001) Seismotectonics of Zimbabwe. African Journal of Science and Technology 1(4). https://doi.org/10.4314/ajst.v1i4.44622

Hutton LK, Boore DM (1987) The ML scale in Southern California. Bulletin of the Seismological Society of America 77:2074–2094. https://doi.org/10.1785/BSSA0770062074

ISC (2022) International Seismological Centre (2022). Online-line Bulletin https://doi.org/doi.org/10.31905/D808B830

Jelsma HA, Dirks PH (2002) Neoarchaean tectonic evolution of the zimbabwe craton. Geological Society, London, Special Publications 199(1):183–211

Kennett BL, Engdahl E, Buland R (1995) Constraints on seismic velocities in the earth from traveltimes. Geophysical Journal International 122(1):108–124. https://doi.org/doi.org/10.1111/j.1365-246X.1995.tb03540.x

Midzi V, Saunders I, Manzunzu B, et al (2018) The 03 april 2017 Botswana M6. 5 earthquake: preliminary results. Journal of African Earth Sciences 143:187–194. https://doi.org/10.1016/j.jafrearsci.2018.03.027

Mulabisana T, Meghraoui M, Midzi V, et al (2021) Seismotectonic analysis of the 2017 Moiyabana earthquake (Mw 6.5; Botswana), insights from field investigations, aftershock and insar studies. Journal of African Earth Sciences 182:104,297. https://doi.org/doi.org/10.1016/j.jafrearsci.2021.104297

Olebetse TA, Mmese ML, Simon RE, et al (2020) Some foreshocks and aftershocks associated with the Moiyabana earthquake of 2017 in Botswana. International Journal of Geosciences 11(4):238–250. https://doi.org/10.4236/ijg.2020.114013

Ottemöller L, Sargeant S (2013) A local magnitude scale ML for the United Kingdom. Bulletin of the Seismological Society of America 103(5):2884–2893. https://doi.org/doi.org/10.1785/0120130085

Ottemöller L, Voss P, Havskov J (2021) Seisan earthquake analysis software for windows, solaris, linux and macosx, version 12.0. 607

Press WH, Teukolsky SA, Vetterling WT, et al (1996) Numerical recipes in fortran 90, 2nd edition

Pujol J (1988) Comments on the joint determination of hypocenters and station corrections. Bulletin of the Seismological Society of America 78(3):1179–1189. https://doi.org/doi.org/10.1785/BSSA0780031179

Richter CF (1935) An instrumental earthquake magnitude scale. Bulletin of the Seismological Society of America 25(1):1–32. https://doi.org/10.1785/BSSA0250010001

Richter CF (1958) Elementary seismology. Seismological Society of America 87(2):474–483

Saunders I, Ottemöller L, Brandt MBC, et al (2013) Calibration of an ML scale for South Africa using tectonic earthquake data recorded by the South African National Seismograph Network: 2006 to 2009. Journal of Seismology 17(2):437–451. https://doi.org/10.1007/s10950-012-9329-0, URL http://link.springer.com/10.1007/s10950-012-9329-0

Storchak DA, Harris J, Brown L, et al (2017) Rebuild of the bulletin of the international seismological centre (isc), part 1: 1964–1979. Geoscience Letters 4(1):1–14

Storchak DA, Harris J, Brown L, et al (2020) Rebuild of the bulletin of the international seismological centre (isc)part 2: 1980–2010. Geoscience Letters 7(1):1–21

Uhrhammer RA, Collins ER (1990) Synthesis of wood-anderson seismograms from broadband digital records. Bulletin of the Seismological Society of America 80(3):702–716. https://doi.org/doi.org/10.1785/BSSA0800030702

Uhrhammer RA, Loper SJ, Romanowicz B (1996) Determination of local magnitude using bdsn broadband records. Bulletin of the Seismological Society of America 86(5):1314–1330. https://doi.org/doi.org/10.1785/BSSA0860051314

Wessel P, Luis J, Uieda L, et al (2019) The generic mapping tools version 6. Geochemistry, Geophysics, Geosystems 20(11):5556–5564. https://doi.org/doi.org/10.1029/2019GC008515

433 # 10 Supplementary materials

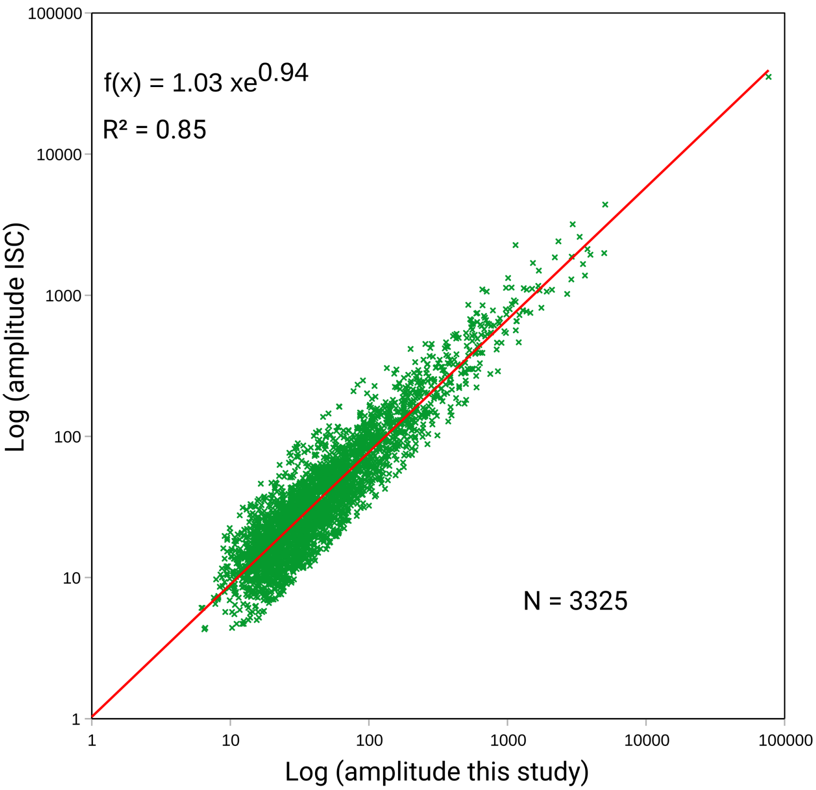

Fig. S1 Log (amplitude) obtained in this study plotted against amplitudes from the ISC Bulletin for LBTB seismic stations.

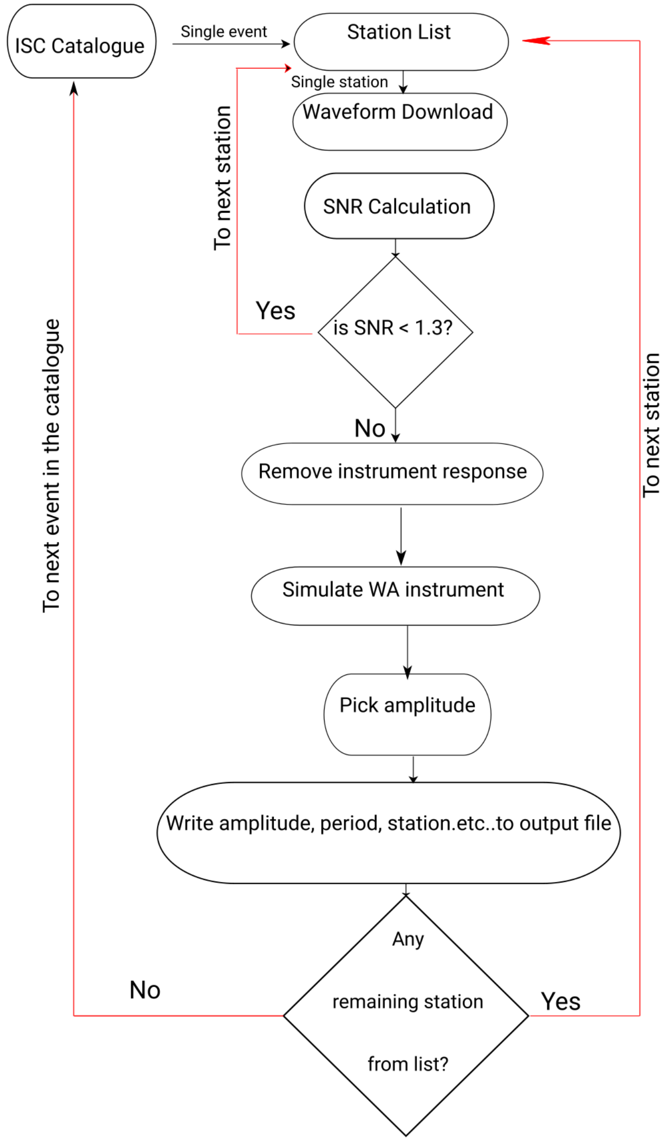

Fig. S2 Flowchart of the procedure we used to pick amplitudes.

Table S1 Station Correction factors with corresponding error at different stations. cf is the Station correction factor, symbol σ represents standard deviation and abbreviation sr denotes the sampling rate. Net is the network and obs represent the number of observation at a seismic station.

No.	Net	Code	Sensor	sr	Lat	Lon	Elev	Obs	cf	σ
1	NR	NE201	STS2	20	-24.51	23.93	980	300	0.32	0.20
2	BX	SKOMA	STS2	40	-24.51	23.93	980	227	0.26	0.19
3	NR	NE202	STS2	20	-24.11	21.78	1153	227	0.07	0.12
4	BX	LKGWB	STS2	40	-24.11	21.78	1153	175	0.02	0.12
5	NR	NE203	STS2	20	-22.99	20.19	1313	127	0.06	0.15
6	BX	KOOLE	STS2	40	-22.99	20.19	1313	127	0.06	0.15
7	NR	NE204	STS2	20	-18.53	21.33	1060	73	-0.18	0.14
8	BX	XAUDM	STS2	40	-18.53	21.33	1060	23	-0.38	0.19
9	NR	NE205	STS2	20	-18.62	23.50	961	89	-0.11	0.21
10	BX	SLIND	STS2	40	-18.62	23.50	961	32	-0.20	0.17
11	NR	NE206	STS2	20	-17.80	25.16	1006	113	0.008	0.26
12	BX	KSANE	STS2	40	-17.80	25.16	1006	89	0.02	0.22
13	NR	NE207	STS2	20	-19.52	21.17	1094	64	0.46	0.17
14	BX	QNGWA	STS2	40	-19.52	21.17	1094	28	0.41	0.18
15	NR	NE208	STS2	20	-21.94	25.44	1083	244	-0.19	0.18
16	BX	KHWEE	STS2	40	-21.94	25.44	1083	157	-0.35	0.21
17	NR	NE209	STS2	20	-21.40	23.77	1005	83	-0.24	0.16
18	BX	CKGRV	STS2	40	-21.40	23.77	1005	117	-0.27	0.20
19	NR	NE210	STS2	20	-21.36	21.21	1198	200	0.24	0.18
20	BX	GRTLG	STS2	40	-21.36	21.21	1198	195	0.10	0.17
21	NR	NE211	STS2	20	-22.85	22.20	1153	352	0.06	0.13
22	BX	KGCAE	STS2	40	-22.85	22.20	1153	231	0.02	0.12
23	NR	NE212	STS2	20	-23.38	24.66	1038	357	0.14	0.29
24	BX	KDWAN	STS2	40	-23.38	24.66	1038	255	0.05	0.17
25	NR	NE213	STS2	20	-25.47	22.85	1030	407	-0.29	0.18
26	BX	PHPEN	STS2	40	-25.47	22.85	1030	150	-0.36	0.20
27	NR	NE214	STS2	20	-19.38	22.16	985	16	-0.11	0.18
28	BX	GMARE	STS2	40	-19.38	22.16	985	34	-0.26	0.25
29	NR	NE215	STS2	20	-18.78	25.19	1035	64	0.14	0.16
30	NR	NE216	STS2	20	-20.19	24.53	956	280	-0.11	0.14
31	BX	PHDHD	STS2	40	-20.19	24.53	956	109	-0.16	0.16
32	NR	NE217	STS2	20	-21.09	27.33	1047	352	0.44	0.18
33	BX	BROLN	STS2	40	-21.09	27.33	1047	354	0.31	0.22
34	NR	NE218	STS2	20	-20.56	26.21	941	376	-0.12	0.16
35	BX	SOOWA	STS2	40	-20.56	26.21	941	221	-0.16	0.17
36	NR	NE219	STS2	20	-22.56	27.44	911	408	-0.20	0.19
37	BX	MREMI	STS2	40	-22.56	27.44	911	243	-0.22	0.21
38	NR	NE220	STS2	20	-23.36	25.85	1020	382	0.47	0.22
39	BX	LPHEP	STS2	40	-23.36	25.85	1020	322	0.39	0.20
40	NR	NE221	STS2	20	-25.81	24.80	1158	540	-0.18	0.22
41	BX	NE221	STS2	40	-25.81	24.80	1158	237	-0.25	0.20
42	XA	SA55	STS2	20	-22.97	28.29	918	279	0.08	0.12
43	XA	SA56	STS2	20	-23.00	29.07	909	569	-0.10	0.09
44	XA	SA57	STS2	20	-22.98	30.02	787	621	0.05	0.08
45	XA	SA63	STS2	20	-23.65	26.08	1008	208	-0.21	0.15
46	XA	SA64	STS2	20	-22.96	26.20	1151	187	-0.08	0.14
47	XA	SA66	STS2	20	-21.90	26.37	1057	184	-0.22	0.14
48	XA	SA67	STS2	20	-21.88	27.27	913	192	0.05	0.09
49	XA	SA70	STS2	20	-21.08	26.33	990	206	-0.06	0.1
50	XA	SA71	STS2	20	-20.92	27.14	1072	153	0.04	0.11
51	XA	SA72	STS2	20	-20.14	28.61	1337	265	0.08	0.13
52	XA	SA73	STS2	20	-21.85	30.27	590	165	-0.03	0.19
53	XA	SA74	STS2	20	-21.92	30.93	487	165	0.13	0.12
54	XA	SA75	STS2	20	-20.86	28.99	971	192	0.04	0.09
55	XA	SA76	STS2	20	-20.63	29.84	978	353	0.01	0.07
56	XA	SA77	STS2	20	-20.75	30.91	576	203	0.03	0.08
57	XA	SA78	STS2	20	-19.46	30.77	1401	224	-0.05	0.09
58	XA	SA79	STS2	20	-20.02	30.51	1078	122	0.03	0.1
59	XA	SA80	STS2	20	-30.97	22.24	1452	130	0.01	0.08
60	AF	BLWY	STS2	40	-20.14	28.61	1348	93	-0.11	0.20
61	XA	MATP	CMG-3T	40	-20.42	28.49	1215	23	-0.16	0.17